An Analysis of Algorithms for In Vivo Fibre Tractography

Jing Li and Burkhard C. Wünsche

University of Auckland, Dept. of Computer Science, Private Bag 92019, Auckland, New Zealand.
Email: burkhard@cs.auckland.ac.nz

Abstract

Diffusion tensor imaging (DTI) is a relatively new imaging technique which is used to measure the water diffusion in the brain. Since water diffusion is influenced by the micro-structure of tissue DTI can be used to identify nerve fibre tracts in the brain. Over recent years many fibre tracking techniques have been proposed, but little work has been done to evaluate and compare these techniques. In this paper we present a framework for designing virtual nerve fibre tracts and for simulating noisy DTI data sets for evaluating and comparing nerve fibre tracking techniques. We have implemented three classes of fibre tractography algorithms, streamlines, tensorlines and tensor deflection, and we devise several error metrics for comparing them. Our analysis shows that all methods are very sensitive to noise and that streamlines fail in regions where nerve fibres cross, whereas tensorlines and tensor deflection cope well with the tested tract topologies.

Keywords: fibre tractography, nerve fibre tracking, diffusion tensor imaging, neuroanatomy, diffusion-weighted MRI

1 Introduction

Diffusion tensor imaging (DTI), also known as *diffusion-weighted MRI imaging* (DWI), is used to measure the intrinsic properties of water diffusion in the brain by an orientation invariant quantity, the diffusion tensor $\mathbf{D}$ [1, 2]. The eigenvalues and eigenvectors of the symmetric second-order tensor $\mathbf{D}$ define the principal axes of a *diffusion ellipsoid* which expresses the spatial distribution of water molecules originating at a point location after an infinitesimal time period.

The directional information of water diffusion in the brain can be used to estimate the structure and the orientation of the never fibre tracts as water tends to diffuse within white matter along the axonal fibre direction in the brain [3]. Due to errors (noise) in the DTI data and because of its low resolution advanced mathematical models must be employed in order to find the fibre tract with the highest probability of being correct. Previously suggested solutions include physically-based models [3, 4], statistical models [5], which make use of the assumption that sudden changes in fibre tract direction are most likely due to errors (noise) in the data, and curvature minimising schemes [6], which are based on the observation that the fibre tracts in a healthy brain usually follow a path with a minimum curvature.

Because of noise and the low sample density of DTI it is usually necessary to smooth, regularise and reconstruct the data before visualising and analysing it. Suitable techniques are described in [7, 8, 9, 10]. Distortions induced by eddy-currents are characterised and corrected in [11, 12]. So far little work has been done to validate, analyse and compare fibre tracking algorithms. Lazar and Alexander have compared fibre tracking algorithms for tensor fields with linear, radial and circular major eigenvector fields [13].

In the following sections we introduce a framework for creating arbitrarily shaped virtual nerve fibre tracts and for simulating noisy DWI data sets from them. We use our framework to evaluate and compare three classes of fibre tractography algorithms.

2 A Framework for Simulating DTI Data

In order to quantitatively compare the fibre tracking algorithms synthetic tensor fields are required [13, 14]. We reconstruct the synthetic tensor fields by first modelling the nerve fibre tracts and surrounding tissue and then determining the directions $\mathbf{e}_i$ and magnitudes λ_i $(i = 1, \ldots, 3)$ of the water diffusion within these structures. The diffusion tensor $\mathbf{D}$ is then given by

$$\mathbf{D}=\begin{pmatrix} d_{xx} & d_{xy} & d_{xz} \\ d_{xy} & d_{yy} & d_{yz} \\ d_{xz} & d_{yz} & d_{zz} \end{pmatrix}=\begin{pmatrix} \mathbf{e}_1 & \mathbf{e}_2 & \mathbf{e}_3 \end{pmatrix}\begin{pmatrix} \lambda_1 & 0 & 0 \\ 0 & \lambda_2 & 0 \\ 0 & 0 & \lambda_3 \end{pmatrix}\begin{pmatrix} \mathbf{e}_1^T \\ \mathbf{e}_2^T \\ \mathbf{e}_3^T \end{pmatrix} \quad (1)$$

2.1 Construction of Virtual Nerve Fibre Tracts

We have developed an interactive user interface which allows the modelling of fibre tract trajectories by B-Spline curves [15]. Virtual nerve fibre tracts are created by fitting a cylindrical surface around the curve as illustrated in figure 1.

In order to determine the principal water diffusions for a point within the nerve fibre tract we define a reference frame for the associated B-Spline curve [16]. The three axes of the reference frame define the principal diffusion directions. The tangent vector is associated with the maximum diffusion value and indicates the direction of the pathway. Since different types of fibre tracts have different ranges of typical diffusivities [17] the user can specify the principal diffusivities accordingly.

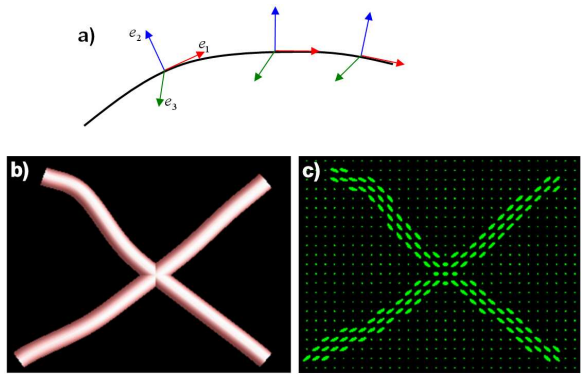

Figure 1: B-Spline curves (a) define the trajectories of fibre tracts (b). The reference frame of the space curves determines the eigenvectors used for computing the synthetic tensor field (c).

2.2 Construction of a Synthetic Tensor Field

In order to obtain a synthetic tensor field for a given set of fibre tracts the user has to specify the number and density of sample points. For each sample point inside a fibre tract we determine the closest curve point to it. We then determine the reference frame at that point and the tract's principal diffusivities and compute the diffusion tensor using equation 1.

If a point is inside several tracts the corresponding tensors are summed up. If a point is outside of all fibre tracts we assume that it lies in a gray matter region and we define an isotropic diffusion tensor using typical values reported in the literature [18].

2.3 Adding Gaussian Noise to DTI Data

To make the synthetic diffusion tensor data more realistic, Gaussian normal noise with zero mean and the standard deviation corresponding to the desired Signal-to-Noise-Ratio (SNR) is added to the real and imaginary channels of the ideal signal for every sample point. The procedure of adding noise to a synthetic tensor field is the reverse of the process for DTI data acquisition [19].

1) Represent the noise-free tensor $\mathbf{D}$, obtained using the procedure described in the previous subsection, by its six independent elements $\mathbf{d} = (d_{xx}, d_{yy}, d_{zz}, d_{xy}, d_{xz}, d_{yz})$.

2) Define six gradient vectors simulating the DTI acquisition scheme:

$$\mathbf{q}_1=\frac{1}{\sqrt{3}}\begin{pmatrix}1\\1\\1\end{pmatrix},\ \mathbf{q}_2=\frac{1}{\sqrt{3}}\begin{pmatrix}-1\\-1\\1\end{pmatrix},\ \mathbf{q}_3=\frac{1}{\sqrt{3}}\begin{pmatrix}1\\-1\\-1\end{pmatrix}$$

$$\mathbf{q}_4=\frac{1}{\sqrt{3}}\begin{pmatrix}-1\\1\\-1\end{pmatrix},\ \mathbf{q}_5=\frac{1}{\sqrt{2}}\begin{pmatrix}1\\1\\0\end{pmatrix},\ \mathbf{q}_6=\frac{1}{\sqrt{2}}\begin{pmatrix}1\\0\\1\end{pmatrix}$$

From this data we can compute the six apparent diffusion coefficients (ADC) as

$$d_i = \mathbf{q}_i^T \mathbf{D} \mathbf{q}_i\ , \quad i = 1, \ldots, 6$$

Let $\hat{\mathbf{d}} = (d_1, d_2, d_3, d_4, d_5, d_6)$ then

$$\hat{\mathbf{d}} = \mathbf{A}\mathbf{d} \quad (2)$$

where $$\mathbf{A}=\frac{1}{3}\begin{pmatrix} 1 & 1 & 1 & 2 & 2 & 2 \\ 1 & 1 & 1 & 2 & -2 & -2 \\ 1 & 1 & 1 & -2 & -2 & 2 \\ 1 & 1 & 1 & -2 & 2 & -2 \\ 1.5 & 1.5 & 0 & 1 & 0 & 0 \\ 1.5 & 0 & 1.5 & 0 & 1 & 0 \end{pmatrix}$$

3) The "ideal" noise-free signals are calculated as [19]

$$S_i = S_0 e^{-bd_i} \quad (3)$$

where S_0 is the base line signal and b is the so-called b-factor. Typical values for b in DTI imaging are $1000 - 1500 s/mm^2$, though some researchers believe that higher values of $3000-4000 s/mm^2$ are needed to resolve more complex fibre connectivity, such as crossing fibre tracts [20].

4) The noise free signals $S = S_i$ $(i = 1, \ldots, 6)$ are treated as complex numbers $Z = a + ib$ where $S = mod(Z) = \sqrt{a^2 + b^2}$. For simplicity we follow Skare et al. [19] and set $a = S$ and $b = 0$ and superimpose independent normal Gaussian noises upon the real and imaginary parts:

$$Z = (S + noise_a) + i(noise_b)$$

where $noise_a$ and $noise_b$ are independent random samples from a Gaussian distribution with mean $\mu = 0$ and a standard deviation σ. The standard deviation is chosen according to the user defined signal to noise ratio $SNR = \frac{S_0}{\sigma}$. Random samples are obtained using the Gaussian random number generator *gasdev* [21].

The resulting noise contaminated signals are

$$S_i = mod(Z) = \sqrt{(S_i + noise_a)^2 + (noise_b)^2}$$

5) The noise contaminated ADCs are calculated using equation 3 and the noisy diffusion tensor is obtained by inverting equation 2.

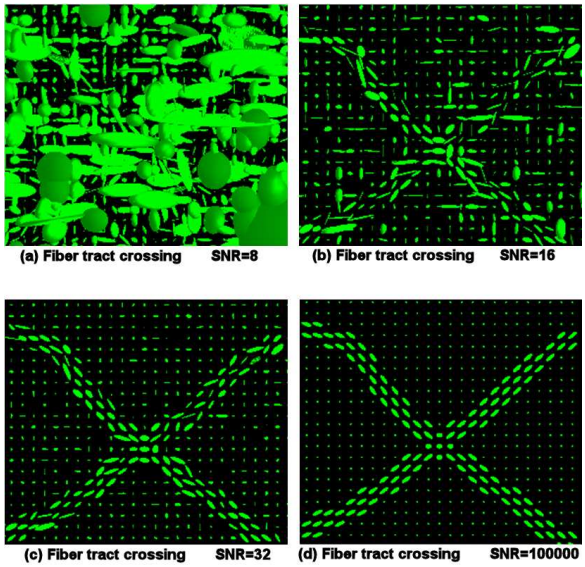

Figure 2: A simulated DTI data set with different SNRs representing crossing fibre tracts.

An example of the resulting simulated noisy DTI data is shown in figure 2. The motivation for this method is given in [19]. Note that it has been shown that MRI data is best modelled with Rician noise, whose distributions, however, are nearly Gaussian for SNRs larger than two [22].

3 Implementation

The simulation framework was implemented in C/C++ using the OpenGL, GLU and GLUT libraries in order to gain platform independence. An object-oriented design makes it easy to add new fibre tracking methods or different types of tensor fields such as real DTI data or fields obtained using different simulation techniques.

3.1 Fibre Tracking Algorithms

We have implemented three types of fibre tracking methods: streamlines, tensorlines and Tensor Deflection (TEND). For all techniques we integrate for a seed point in both the positive and negative eigenvector direction. The tracking continues until the boundary of the data set is reached or the mean diffusivity λ_{mean} and diffusion anisotropy λ_{aniso} at the current curve point lie outside a previously specified admissible range of values [23].

Let $\mathbf{D}$ be the diffusion tensor and $\mathbf{e}_i$ and λ_i $(i = 1, \ldots, 3)$ be its eigenvectors and eigenvalues, respectively, with $\lambda_1 \geq \lambda_2 \geq \lambda_3$. A nerve fibre can be computed as a *streamline* $\mathbf{S}(t)$ of the major eigenvector field, i.e., it is the solution of the ordinary differential equation

$$\frac{d\mathbf{S}(t)}{dt} = \mathbf{e}_1(\mathbf{S}(t)) \ , \quad \mathbf{S}(0) = s_0$$

where s_0 is the seed point. We solve this equation using a 4^{th} order Runge-Kutta method [21].

The *tensor deflection* (TEND) fibre tracking method uses the entire diffusion tensor information to deflect the current fibre direction $\mathbf{v}_{in}$ [24]. For each integration step the new fibre direction is computed from the diffusion tensor as $\mathbf{v}_{out} = \mathbf{D}\mathbf{v}_{in}$.

The *tensorline* tracking technique from Weinstein et al. is a mixture of the two previously described techniques [25]. It not only considers the principal diffusion direction of the local tensor, but also the nearby orientation information of the local tensor by adding an advection term in a standard diffusion-based propagation method.

$$\mathbf{v_{new}} = c_l\mathbf{e}_1 + (1 - c_l)((1 - w)\mathbf{v}_{in} + w\mathbf{v}_{out})$$

where $c_l = (\lambda_1 - \lambda_2)/(\lambda_1 + \lambda_2 + \lambda_3)$ is the linear anisotropy coefficient and w is a user-defined weighting term which we set to $w = 0.2$ as recommended in [25].

3.2 Error Metrics

In order to analyse a fibre tracking method the user draws one or several nerve fibres and creates a DTI data set with the desired SNR from it. The user then defines a set of seed points by specifying a region of interest and/or an admissible range of values for the mean diffusivity λ_{mean} and diffusion anisotropy λ_{aniso} [23].

For each seed point we track a nerve fibre using the methods described in the previous section. In order to analyse the results we have to define what constitutes a correct solution. We choose as correct solution the B-Spline curve defining the trajectory of the nerve fibre tract and translate it linearly with respect to its reference frame such that it passes through the given seed point.

In order to evaluate the quality of a fibre tracking method we introduce three error metrics:

1. The average length of the simulated nerve fibres. This error measure shows how stable a tracking method is with regard to small perturbations which can cause a computed nerve fibre to leave a fibre tract.

2. The number of computed fibres which stay within the correct fibre tract. This error measure shows how stable the tracking method is in regions of crossing or adjacent fibre tracts.

3. The least square distance error (LSE) of the computed nerve fibres with respect to the correct solution. This error measure is computed for the part of a simulated nerve fibre which lies within the correct fibre tract and it indicates the precision of a fibre tracking algorithm.

4 Results

We evaluated the suitability of streamlines (ST), tensorlines (TL) and tensor deflection (TEND) for fibre tractography using simulated DTI data sets for two scenarios: two crossing fibre tracts as illustrated in figure 2 and a branching fibre tract.

4.1 Crossing Fibre Tracts

The results for tracking two crossing fibre tracts are shown in the figures 3-5. The horizontal axis specifies the minimum length of nerve fibres considered for computing the error measure.

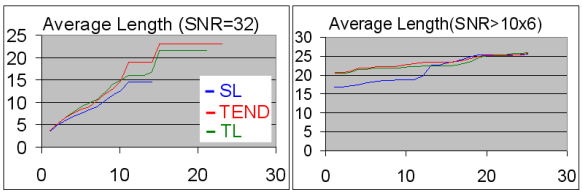

Figure 3: The average length of nerve fibres computed using streamlines (ST), tensorlines (TL) and tensor deflection (TEND).

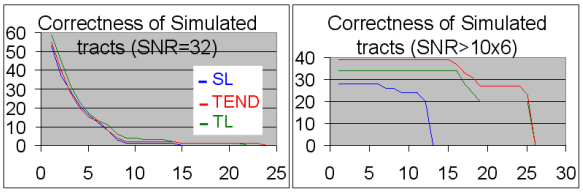

Figure 4: The number of nerve fibres computed using streamlines (ST), tensorlines (TL) and tensor deflection (TEND), which lie completely within the correct fibre tract.

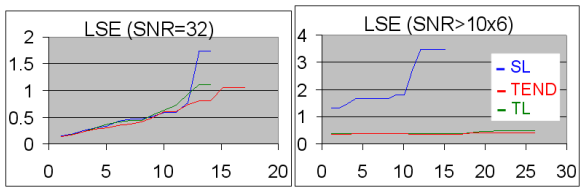

Figure 5: The average least square error of nerve fibres computed using streamlines (ST), tensorlines (TL) and tensor deflection (TEND).

Since all seed points are inside of fibre tracts the expected length of all computed nerve fibres is equal to the length of a fibre tract (≈ 23 units). It can be seen that for SNR=32 most computed nerve fibre trajectories, independent of the tracking method used, swerve outside the fibre tract. A more detailed examination reveals that the closer a seed point is to the boundary of the fibre tract the more likely the tracking method is to fail. Overall the tensor deflection method results in the longest fibres for low signal to noise ratios. If noise is virtually eliminated all methods perform reasonable well and the lengths of the computed nerve fibres are close to the expected value.

Figure 4 shows the correctness of the computed nerve fibres, i.e., whether the nerve fibres lie entirely within one fibre tract or whether they diverge into the wrong tract in the region where the fibre tracts cross. It can be seen that for SNR=32 all tracking methods fail. If noise is virtually eliminated the streamline method always diverges into the wrong fibre track, whereas the tensor deflection method stays in most cases within the fibre tract where it started.

The precision of the three algorithms for SNR=32 is similar for all tracking methods and the derivation from the correct result increases approximately linear with the length of a nerve fibre. If noise is virtually eliminated the precision of the tensorline and tensor deflection method improve considerably whereas the streamline method gets slightly worse.

4.2 Branching Fibre Tracts

The results shown in the figures 6-8 demonstrate that all of the three tracking methods perform well for branching fibre tracts, but are again very sensitive to noise.

Our results indicate that overall tensor deflection is the best nerve fibre tracking method, in particular if we deal with crossing fibre tracts which are common in real DTI data sets. The streamline method performs well for branching topologies but fails for crossing fibre tracts because it only considers

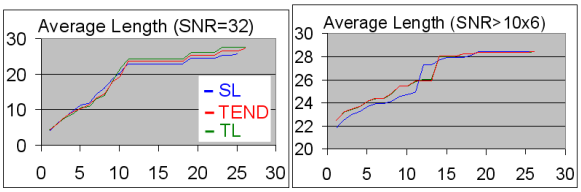

Figure 6: The average length of nerve fibres computed using streamlines (ST), tensorlines (TL) and tensor deflection (TEND).

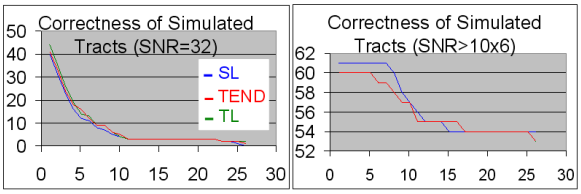

Figure 7: The number of nerve fibres computed using streamlines (ST), tensorlines (TL) and tensor deflection (TEND), which lie completely within the correct fibre tract.

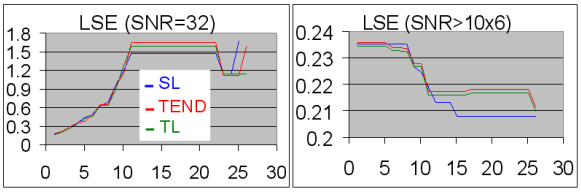

Figure 8: The average least square error of nerve fibres computed using streamlines (ST), tensorlines (TL) and tensor deflection (TEND).

the major eigenvector. As a result the method is not able to track nerve fibres in regions of planar anisotropic diffusion ($\lambda_1 \approx \lambda_2$).

5 Conclusion

We have introduced a framework for simulating DTI data and for testing and analysing fibre tracking methods. Our tool allows the user to define virtual nerve fibre tracts by B-Spline curves, which specify the direction of the pathway, and a radius which specifies the thickness of the tract.

A DTI data set is simulated by computing for each sample point and each fibre tract typical diffusion values according to the fibre tract direction at that point. The contributions of each tract at a sample point are summed up and complex Gaussian normal noise with zero mean and the standard deviation corresponding to a user-defined SNR is added. The procedure of adding noise to a synthetic tensor field is the reverse of the process for DTI data acquisition.

We have used our framework to analyse and compare three fibre tracking techniques and we found that overall the tensor deflection methods performs best, whereas the streamline method fails completely for crossing fibre tract topologies. The tensorline method represents a mixture of these two techniques and performs slightly worse than tensor deflection but considerable better than the streamline technique.

In future work we want to investigate other fibre tract topologies, add modelling capabilities for simulating other anatomical structures (e.g., cerebral spinal fluid) and simulate pathological DTI data (e.g., after a subcortical stroke). Furthermore we want to investigate alternative fibre tracking methods such as [3, 4, 6].

References

[1] P. J. Basser, J. Mattiello, and D. L. Bihan, "MR diffusion tensor spectroscopy and imaging," *Biophysical Journal*, vol. 66, pp. 259–267, 1994.

[2] P. J. Basser, "Inferring microstructural features and the physiological state of tissues from diffusion-weighted images," *NMR in Biomedicine*, vol. 8, no. 7–8, pp. 333–344, 1995.

[3] P. J. Basser, S. Pajevic, C. Pierpaoli, J. Duda, and A. Aldroubi, "In vivo fiber tractography using DT-MRI data," *Magnetic Resonance in Medicine*, vol. 44, pp. 625–632, Oct. 2000. URL: `http://dir2.nichd.nih.gov/nichd/limb/stbb/invivofiber.pdf`.

[4] D. S. Tuch, T. G. Reese, M. R. Wiegell, N. Makris, J. W. Belliveau, and J. van Wedeen, "High angular resolution diffusion imaging reveals intravoxel white matter fiber heterogeneity," *Magnetic Resonance in Medicine*, vol. 48, pp. 577–582, Oct. 2002.

[5] C. Poupon, J.-F. Mangin, V. Frouin, J. Régis, F. Poupon, M. Pachot-Clouard, D. L. Bihan, and I. Bloch, "Regularization of MR diffusion tensor maps for tracking brain white matter bundles," in *Medical Image Computing and Computer-Assisted Intervention - MICCAI '98*, pp. 489–498, Springer Verlag, Oct. 1998.

[6] C. Poupon, C. A. Clark, V. Frouin, J. Régis, I. Bloch, D. Le Bihan, and J.-F. Mangin, "Regularization of diffusion-based direction maps for the tracking of brain white matter fascicles," *Neuroimage*, vol. 12, pp. 184–195, Aug. 2000.

[7] A. Aldroubi and P. J. Basser, "Reconstruction of vector and tensor fields from sampled discrete data," in *The Functional and Harmonic Analysis of Wavelets and Frames*, vol. 247 of *Contemporary Mathematics*, pp. 1–15, American Mathematical Society, 1999. URL: `http://atlas.math.vanderbilt.edu/~aldroubi/dtmri.ps`.

[8] C.-F. Westin, S. E. Maier, B. Khidir, P. Everett, F. A. Jolesz, and R. Kikinis, "Image processing for diffusion tensor magnetic resonance imaging," in *Medical Image Computing and Computer-Assisted Intervention - MICCAI '99*, pp. 441–452, Springer Verlag, Sept. 1999.

[9] K. Hahn, S. Prigarin, and B. Pütz, "Edge preserving regularization and tracking for diffusion tensor imaging," in *Medical Image Computing and Computer-Assisted Intervention - MICCAI '01*, pp. 195–203, Springer Verlag, Oct. 2001.

[10] D. Xu, S. Mori, D. Shen, and C. Davatzikos, "Statistically-based reorientation of diffusion tensor fields," in *Proceedings of the IEEE Symposium on Biomedical Imaging*, (Washington D.C., 7–10 July), pp. 757–760, July 2002. URL: `http://oasis.rad.upenn.edu/~dgshen/papers/Dongrong_ISBI2002.pdf`.

[11] P. Jezzard, A. S. Barnett, and C. Pierpaoli, "Characterization of and correction for eddy current artifacts in echo planar diffusion imaging," *Magnetic Resonance in Medicine*, vol. 39, pp. 801–812, May 1998.

[12] J. F. Mangin, C. Poupon, C. Clark, D. L. Bihan, and I. Bloch, "Eddy-current distortion correction and robust tensor estimation for MR diffusion imaging," in *Medical Image Computing and Computer-Assisted Intervention - MICCAI '01*, pp. 186–194, Springer Verlag, Oct. 2001.

[13] M. Lazar and A. L. Alexander, "An error analysis of white matter tractography methods: synthetic diffusion tensor field simulations," *NeuroImage*, vol. 20, pp. 1140–1153, Oct. 2003.

[14] L. Jonasson, X. Bresson, P. Hagmann, O. Cuisenaire, R. Meuli, and J.-P. Thiran, "White matter fiber tract segmentation in DT-MRI using geometric flows," *Medical Image Analysis*, vol. 9, pp. 223–236, June 2005.

[15] J. Hoschek and D. Lasser, *Fundamentals of Computer Aided Geometric Design*, ch. 14, pp. 572–601. Wellesley, MA: AK Peters, 2^{nd} ed., 1992.

[16] J. Bloomenthal, "Calculation of reference frames along a space curve," in *Graphics Gems Vol. 1*, pp. 567–571, San Diego, CA, USA: Academic Press Professional, Inc., 1990. URL: `http://www.unchainedgeometry.com/jbloom/pdf/ref-frames.pdf`.

[17] N. G. Papadakis, D. Xing, C. L.-H. Huang, L. D. Hall, and T. A. Carpenter, "A comparative study of acquisition schemes for diffusion tensor imaging using MRI," *Journal of Magnetic Resonance*, vol. 137, pp. 67–82, Mar. 1999.

[18] C. Pierpaoli, P. Jezzard, P. J. Basser, A. Barnett, and G. D. Chiro, "Diffusion tensor MR imaging of the human brain," *Radiology*, vol. 201, pp. 637 – 648, Dec. 1996.

[19] S. Skare, T.-Q. Li, B. Nordell, and M. Ingvar, "Noise considerations in the determination of diffusion tensor anisotropy," *Magnetic Resonance Imaging*, vol. 18, pp. 659–669, July 2000.

[20] D. S. Tuch, "Q-ball imaging," *Magnetic Resonance in Medicine*, vol. 52, pp. 1358–1372, Dec. 2004.

[21] W. H. Press, W. T. Vetterling, S. A. Teukolsky, and B. P. Flannery, *Numerical Recipes in C - The Art of Scientific Computing*. Cambridge University Press, 2^{nd} ed., 1992.

[22] H. Gudbjartsson and S. Patz, "The rician distribution of noisy MRI data," *Magnetic Resonance in Medicine*, vol. 34, pp. 910–914, Dec. 1995.

[23] B. C. Wünsche and R. Lobb, "The 3D visualization of brain anatomy from diffusion-weighted magnetic resonance imaging," in *Proceedings of GRAPHITE 2004*, pp. 74–83, ANZGRAPH and SEAGRAPH, 2004.

[24] M. Lazar, D. M. Weinstein, J. S. Tsuruda, K. M. Hasan, K. Arfanakis, M. E. Meyerand, B. Badie, H. A. Rowley, V. Haughton, A. Field, and A. L. Alexander, "White matter tractography using diffusion tensor deflection," *Human Brain Mapping*, vol. 18, pp. 306–321, Apr. 2003.

[25] D. Weinstein, G. Kindlmann, and E. Lundberg, "Tensorlines: Advection-diffusion based propagation through diffusion tensor fields," in *Proceedings of Visualization '99*, pp. 249–253, IEEE, Oct. 1999.